Materials Advances

ROYAL SOCIETY OF CHEMISTRY

PAPER

View Article Online
View Journal | View Issue

Cite this: *Mater. Adv.*, 2025, **6**, 7958

Sonochemical synthesis of MOF-235 and polyvinylpyrrolidone (PVP)-assisted phase transformation to MIL-53(Fe)

Farnaz Shammiry and Alejandro Montesinos-Castellanos *

Metal–organic frameworks (MOFs) have garnered significant interest due to their diverse applications in industry, synthetic chemistry, and biomedicine. However, achieving MOF materials through fast and facile methods remains challenging due to the frequent formation of mixed phases, which can lead to misassignment of phase structures and complicated characterization. To overcome these challenges, the development of alternative synthesis strategies is required. In this study, a rapid and straightforward sonochemical method was employed to synthesize MOF-235 as an iron-based MOF. During the synthesis, polyvinylpyrrolidone (PVP) was applied as a surfactant to influence the physicochemical properties of MOFs. Surprisingly, the results demonstrated that the combination of ultrasound and PVP not only modified the physicochemical properties of MOFs but also induced a phase transformation from MOF-235 to MIL-53(Fe), resulting in a more stable structure within a short period of synthesis and at a constant temperature. Notably, this is the first report identifying PVP as a surfactant capable of driving a structural phase transition in MOF-235. This strategy promoted surface modification, changed textural properties and resulted in more uniform particle distribution. These findings provide a promising route to achieve better phase control in MOF synthesis and offer insights into surfactant-assisted phase engineering.

Received 1st July 2025,
Accepted 2nd September 2025

DOI: 10.1039/d5ma00699f

rsc.li/materials-advances

Introduction

Decades of research have demonstrated the exceptional properties of metal organic frameworks (MOFs). However, their widespread commercial adoption remains limited due to challenges related to stability, scalability, and practical implementation. Although more than 100 000 MOFs have been reported and over 500 000 structures have been predicted, their high complexity and unpredictable behavior continue to pose challenges for commercial MOF production.[1] MOFs are hybrid materials that exhibit remarkable structural flexibility due to their tunability during synthesis. Recently, research has focused on discovering or optimizing MOFs by adjusting reactants and synthesis parameters (*e.g.*, energy source, temperature, reaction time, and molar ratios).[2] However, their sensitivity to these factors resulted in unpredictable behavior and structural complexity, which made it difficult to follow the general protocol of synthesis.[3] Moreover, the complexity and incomplete synthesis protocols in the literature pose challenges, such as unsatisfactory or unexpected results for the product.[4]

Iron-based MOFs, among the diverse range of MOFs, have attracted considerable interest due to their cost-effectiveness for large-scale production, high surface area, and excellent biocompatibility.[5] For instance, in biomedical applications, MIL-100(Fe) has demonstrated the lowest toxicity and the highest biocompatibility compared to other MOFs.[6] Similarly, MIL-101(Fe) exhibits a high drug-loading capacity, accommodating up to 1.4 g of ibuprofen per g of MOF for drug delivery.[7] Furthermore, iron-based MOFs have shown promise in environmental applications as well.[8] For example, incorporating NH_2-MIL-101(Fe) with other photocatalytic materials has significantly enhanced hydrogen production through photocatalytic water splitting, achieving a rate of 954 μmol h^{-1} and yielding 2770 μmol of hydrogen in pure water.[9]

Among iron-based MOFs, MIL-53(Fe) stands out due to its unique flexible porous structures, which exhibit "breathing behavior" a property that makes dynamic changes in pore size in response to external stimuli.[10,11] Additionally, MIL-53(Fe) is known as a thermodynamically stable material, which has been identified as the thermodynamically favored product of MOF-235.[12] The successful synthesis of MIL-53(Fe) has traditionally been achieved through conventional methods, which involve the initial formation of MOF-235, followed by its dissolution and recrystallization at high temperatures or extended reaction

Tecnologico de Monterrey, Institute of Advanced Materials for Sustainable Manufacturing, Ave. Eugenio Garza Sada 2501 Sur, Col: Tecnologico, Monterrey, NL, 64700, Mexico. E-mail: alejandro_montesinos@tec.mx

times. For example, Bara *et al.* demonstrated that MIL-53(Fe) can be obtained using a conventional method after more than one week of synthesis at 120 °C or within two days at 150 °C.[13] However, these synthesis methods present several drawbacks, including challenges in changing or controlling the size and surface morphology of MIL-53(Fe).

To address these challenges, researchers have explored various synthesis strategies to improve the efficiency, bioavailability, and self-assembly of MIL-53(Fe). However, the absence of clearly defined synthesis protocols and inaccurate crystallographic characterization has frequently led to phase misidentification and structural confusion regarding the differences between MOFs.[14] For instance, Haque *et al.* and Gordon *et al.* investigated the effect of rapid nucleation methods on the synthesis of MIL-53(Fe).[15,16] They reported that smaller and more homogeneous MOF particles were synthesized in 7 minutes using ultrasound irradiation (acoustic cavitation). However, XRD analysis revealed that the resulting crystal structure did not correspond to MIL-53(Fe) and indicated a different phase, as discussed by other authors.[13,17] This discrepancy highlights the challenges associated with phase evolution during MOF synthesis. While these studies attempted to explain the issue through classical nucleation and growth mechanisms, they did not fully account for the high sensitivity of MOFs to synthesis parameters. As a result, the structural transformation of MOFs remains difficult to predict using general crystallization models, such as LaMer's model.

In this sense, various studies have shown that phase engineering in metal–organic frameworks (MOFs) could open new strategies to manipulate MOF structures and features. Various general frameworks based on acid–base and coordination chemistry have been described and proposed for adjusting the crystal size and growth or phase transformation of the MOFs.[18,19] However, modulators have exhibited a significant impact not only on phase transformations but also on the physicochemical properties of MOFs. The structure of MOFs is constructed from metals and linkers and their physicochemical properties such as particle size are governed by a competition between particle growth, driven by diffusing metal ions, and particle termination, caused by the depletion of local metal ion concentrations through rapid ligand complexation.[20] On the other hand, kinetically favored phases tend to crystallize at relatively low precursor concentrations, whereas thermodynamically stable phases typically require higher concentrations for their formation, as previously discussed.[21,22] Therefore, the choice of suitable modulators can influence nucleation and phase transformation.

Different types of modulators, such as organic acids and polymeric materials, have been employed to tune MOF synthesis.[23] For example, increasing acetic acid concentration in the solvothermal reaction between $FeCl_3$ and H_2BDC has been shown to induce a phase transition from MOF-235 to MIL-88B(Fe), highlighting the role of modulators in directing phase formation.[13,19] While acids are effective modulators for MOFs, certain non-ionic polymers such as polyvinylpyrrolidone (PVP) can act as both a modulator and a surfactant due to their unique structure and hydrophobic properties.[24] For instance, Li *et al.* demonstrated the hydrothermal synthesis of MIL-53(Fe) with the cooperation of PVP as a surfactant to reduce particle size (from ~2 μm to ~500 nm).[25] In another study, Wang *et al.* investigated the effect of different amounts of PVP on the synthesis of MOF-199. Their results indicated that PVP successfully acted as a nucleating agent, leading to a reduction in particle size, and as a coordinating agent, facilitating the formation of larger pores.[26]

Although modulators have been successfully employed to tune the structural properties of MOFs, most of these studies have relied on conventional synthesis methods that require extended reaction times, high pressures, and significant energy input. Therefore, expanding design principles is essential to achieve precise control over the crystal phase formation and obtain thermodynamically stable structures, thereby enabling the integration of MOFs into various applications.[23]

Ultrasound-assisted synthesis has emerged as an alternative approach for enhancing nucleation and crystallization rates. This technique generates intense localized pressure and heat through acoustic cavitation, facilitating linker deprotonation and metal–ligand interactions. As a result, ultrasound enables the formation of smaller particles within a significantly shorter reaction time.[27] For instance, Son *et al.* synthesized MOF-5 particles that were 60 times smaller in just 30 minutes using ultrasound, compared to 24 hours required by conventional methods.[28] Similarly, Chalati *et al.* successfully synthesized MIL-88A in approximately 15 minutes, whereas the conventional approach took 24 hours.[29] Additionally, Amaro-Gahete *et al.* reported that the sonochemical method positively influenced the morphology, surface area, and porosity of MIL-88A particles, achieving synthesis in just 1 hour.[30]

Despite these advantages, ultrasound-assisted synthesis has certain limitations, such as lower crystallinity and yield, as well as the formation of mixed-phase frameworks. However, incorporating modulators during synthesis likely presents a promising strategy to address these challenges. So far, the combined use of different modulators such as tannic acid, polyvinylpyrrolidone (PVP), polyethylene glycol (PEG), and other types of polymers during ultrasound synthesis has remained largely unexplored. Therefore, further studies are required to investigate their potential in enabling phase modification and improving the overall performance of MOFs for targeted applications.

In this study, an ultrasound-assisted synthesis method was employed to synthesize MOF materials at a constant temperature of 70 °C. First of all, a suitable synthesis time was determined to achieve high crystallinity of MOF-235(Fe) using the sonochemical method. Furthermore, polyvinylpyrrolidone (PVP) as a synergetic modulator was used during the synthesis to adjust the size and shape, also to induce phase transformation of MOFs. The effects of PVP incorporation were analyzed through various characterization techniques, including X-ray diffraction (XRD), scanning electron microscopy (SEM), Fourier-transform infrared (FTIR) spectroscopy, dynamic light scattering (DLS), and nitrogen adsorption measurements.

Experimental

Materials

All the chemicals were used as purchased without any further purification. Terephthalic acid (H_2BDC, 98%), iron chloride hexahydrate ($FeCl_3{\cdot}6H_2O$, $\geq$99%), *N*,*N*-dimethylmethanamide (DMF $\geq$ 99.8%), polyvinylpyrrolidone K30 (PVP), and methanol (CH_3OH, 99.9%) were purchased from Sigma-Aldrich Company.

Synthesis PVP-0/MM and PVP-0/MW

MOFs were synthesized following the conventional synthesis method reported before.[13] First, terephthalic acid (12 mmol) was dissolved in 60 mL of DMF and stirred for 10 minutes (solution I). Then, iron(III) chloride hexahydrate (12 mmol) was added to solution I, and the mixture was stirred for an additional 20 minutes to obtain solution II. This solution was then transferred to a reactor equipped with an ultrasonic probe (VCX 750, Sonics & Materials, Inc.) and sonicated for 2, 4 and 6 hours at 33% power (20 kHz, 750 W maximum power output). The reaction temperature was maintained at approximately 70 °C ± 1 °C using a circulating water bath. After completion of the reaction, the ultrasound probe was turned off, and the mixture was allowed to cool to room temperature. The resulting suspension was first separated then washed with methanol by centrifugation at 13 000 rpm (25 °C), and the PVP-0/M solid was obtained.

Post-synthesis treatment of PVP-0/M samples

PVP-0/MM. The PVP-0/M sample was washed two more times with methanol and centrifuged again at 13 000 rpm (25 °C). The final solid was re-dispersed in methanol using an ultrasonic bath, transferred to a beaker, and dried in an oven at 160 °C for 15 hours (1 atm under air). The resulting sample was labelled as PVP-0/MM.

PVP-0/MW. The PVP-0/M sample was washed two more times with deionized water and centrifuged again at 13 000 rpm (25 °C). The final solid was re-dispersed in deionized water using an ultrasonic bath, transferred to a beaker, and dried in an oven at 160 °C for 15 hours (1 atm under air). The resulting sample was labelled as PVP-0/MW.

Synthesis of PVP-*x*/MM and PVP-*x*/MW

The PVP-modulated MOFs were synthesized using the same procedure as above, with the addition of various amounts of PVP. First, terephthalic acid (12 mmol) was dissolved in 60 mL of DMF and stirred for 10 minutes (solution I). Then, iron(III) chloride hexahydrate (12 mmol) was added to solution I, and the mixture was stirred for 10 minutes to obtain solution II. Different amounts of PVP (21, 43, 86, 129, and 173 mmol), corresponding to H_2BDC : PVP molar ratios of 1 : 0.25, 1 : 0.5, 1 : 1, 1 : 1.5, and 1 : 2, were added to solution II and stirred for another 10 minutes to obtain solution III. Solution III was then transferred to the ultrasound equipment and reacted under the same conditions described above (33% power, 70 °C, 20 kHz, 750 W) for 6 hours. After cooling to room temperature, the suspension was separated and washed with methanol by centrifugation at 13 000 rpm (25 °C), and the PVP-*x*/M solid was obtained.

Post-synthesis treatment for PVP-*x*/M samples

The post-synthesis treatments for PVP-*x*/M samples followed the same procedures described for PVP-0/M. The PVP-*x*/M sample was washed two more times with either methanol or deionized water and centrifuged again at 13 000 rpm (25 °C). The final solid was then re-dispersed using an ultrasonic bath and dried in an oven at 160 °C for 15 hours (1 atm under air). The resulting samples were labelled as PVP-*x*/MM (methanol-treated) and PVP-*x*/MW (water-treated), respectively. For instance, PVP-1/MW refers to the sample synthesized with an H_2BDC : PVP molar ratio of 1 : 1 and subjected to post-synthesis treatment using deionized water.

Characterization

To investigate the properties of the samples X-ray diffraction (XRD) patterns were recorded using a Panalytical model Empyrean diffractometer, and Cu Kα (0.154 nm) radiation. Fourier-transform infrared spectroscopy was carried out using a PerkinElmer Frontier spectrometer in the wavelength range of 4000 to 400 cm^{-1}. The nitrogen adsorption–desorption isotherm was obtained with a NOVA Touch LX1 at −196 °C. In each case, the sample was vacuum-dried at 120 °C for 12 h before analysis. The morphology of the materials was determined by scanning electron microscopy (Zeiss EVO MA25 microscope). Dynamic light scattering analysis (Nanobrook 90 Plus Pals) was employed to measure the average particle size distribution.

Results and discussion

Characterization of the sonochemical synthesis

In this study, ultrasound irradiation was employed as an efficient and rapid alternative to conventional synthesis methods. However, according to the available literature, there is a lack of discussion regarding the suitable reaction time to synthesize MOFs using the sonochemical method. Therefore, in this work, MOFs were synthesized using an ultrasonic probe in 2, 4, and 6 hours at a constant temperature of 70 °C to determine the effect of reaction time on the final product.

To analyze the chemical interactions between functional groups, Fourier-transform infrared (FT-IR) spectroscopy was used (Fig. 1). Since no significant differences or additional peaks were observed in the FTIR spectra of samples with water and methanol post-synthesis treatment, only the FTIR results of the methanol-treated samples are presented here for conciseness.

The FT-IR spectra of the PVP-0/MM samples synthesized *via* ultrasound-assisted methods at 2–6 hours, compared to the H_2BDC linker spectrum, showed characteristic peaks at 1660, 1592, 1388, 750, and 550 cm^{-1}, revealing the formation of MOF-235, aligning with previous studies that employed conventional methods.[12,31] The appearance of a vibrational peak at around 550 cm^{-1} confirmed the formation of Fe–ligand bonds.

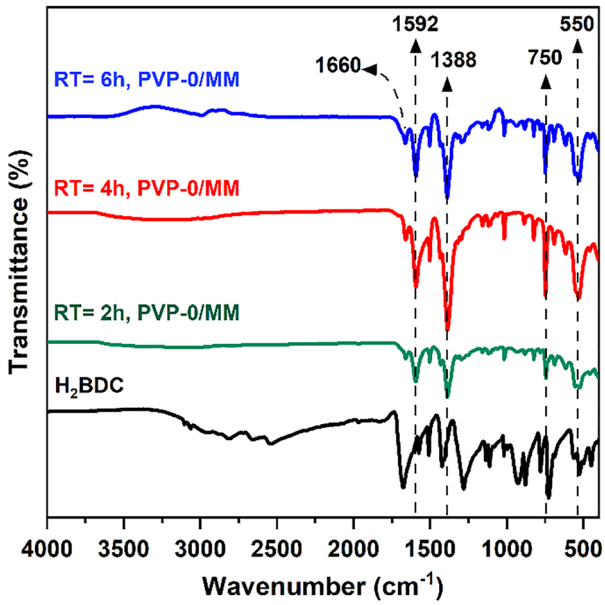

Fig. 1 FTIR spectra of MOF samples (PVP-0) synthesized in 2–6 h using an ultrasound probe at a constant temperature of 70 °C. RT = reaction time.

The peak at 750 cm^{-1} is related to C–H bending vibrations of the benzene ring, belonging to terephthalic acid. The intense peaks at 1592 and 1388 cm^{-1} were assigned to the asymmetric (ν_{as}(C–O)) and symmetric (ν_s(C–O)) stretching vibrations, confirming the presence of the dicarboxylate group within the solids. Additionally, the peak at 1660 cm^{-1} was associated with the (C═O) group of the H_2BDC linker.[32]

X-ray diffraction (XRD) analysis was used to assess the crystalline phase of MOFs, synthesized in 2, 4 and 6 hours (Fig. 2). The samples synthesized in 2 hours exhibited several intense peaks at approximately 9°, 12.4°, 17°, 18.5° and 27.5°, some of which correspond to the precursor materials, such as protonated H_2BDC and $FeCl_3$ labelled in Fig. 2.[33–35] The XRD patterns of H_2BDC and $FeCl_3$ are provided in the SI. The XRD pattern of the sample synthesized in 4 hours showed very low peak intensities, suggesting that no distinct Fe-MOF phase had formed. To obtain materials with higher quality for characterization, post-synthesis treatment was performed using two polar solvents, water (dielectric constant ~80) and methanol (~33). This purification step aimed to wash the particles and remove free linker molecules and residual solvent from the pores or surfaces of the particles synthesized using an ultrasound probe for 6 hours.[3] After post synthesis treatment, the samples synthesized in 6 hours displayed well-defined diffraction peaks at 9.42° (101), 12.58° (102), 16.18° (200), 18.86° (202), 19.30° (004), and 22.02° (3–11), closely matching the reference pattern of MOF-235 (CIF: 255079), synthesized *via* the solvothermal method.[31]

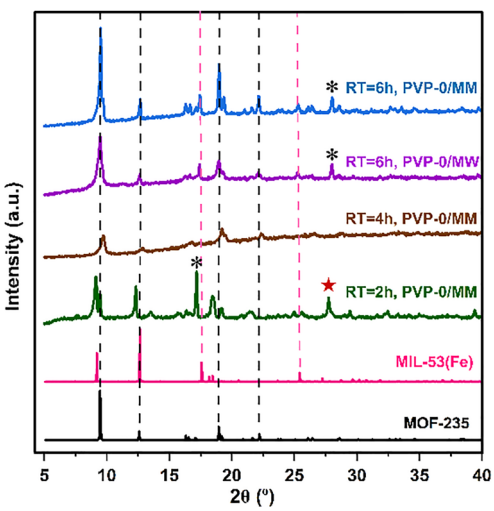

Fig. 2 XRD patterns of MOF samples (PVP-0) synthesized in 2–6 h using an ultrasound probe (70 °C). RT = Reaction time. The MOF-235 and MIL-53(Fe) patterns were recorded from CIF files of MOF-235 and MIL-53(Fe).[31,36] The unreacted $FeCl_3$ (★) and H_2BDC (*) phases were marked in the patterns.[33,34]

While the sample synthesized in 6 hours compared to 4 hours showed higher crystallinity, minor peaks at 17.4°, 25.2°, and 28° were observed. This observation might be evidence for the formation of a second crystalline phase structure due to extreme cavitation conditions of ultrasound or the presence of unreacted materials as well.

To get further insights, the XRD results of the samples were compared with various crystal phases of iron-based MOFs. The diffraction peaks around 2θ = ~9.4°, 12.5°, 17.5°, and 25° closely matched the reference pattern of MIL-53(Fe) (a = 19.31 Å, b = 15.03 Å, c = 6.83 Å, β = 96.3°, V = 1973.5 $Å^3$),[36] although peaks at 2θ = 9.4° and 12.5° overlapped with the 9.42° (101) and 12.58° (102) peaks, belonging to MOF-235.

On the other hand, the peak at 28° (marked by asterisks) was probably related to the presence of an unreacted linker (H_2BDC).[35] This hypothesis could be proved with slight differences observed in the XRD patterns related to the intensities of characteristic peaks between PVP-0/MM (methanol-treated) and PVP-0/MW (water-treated) samples. The intensity of the main peaks compared to the unreacted material peaks in the PVP-0/MM sample was higher than in PVP-0/MW. This might be associated with the lower solubility of terephthalic acid in water (0.0017 g/100 g solvent at 25 °C) compared to methanol (0.1 g/100 g solvent at 25 °C), as reported previously.[37] Consequently, the presence of a peak at 28° is related to the presence of an unreacted linker, which was washed and removed better during post-synthesis treatment with methanol than with water. According to the XRD and FTIR results, in this study, crystalline MOF-235 was successfully synthesized using an ultrasound probe in 6 hours at a constant temperature of 70 °C, which is lower than the temperature typically reported for conventional methods (≥120 °C).[13] This could be due to the cavitation phenomenon of sonochemical synthesis, which can promote rapid MOF crystallization.[38]

However, the sonochemical synthesis conditions may also influence the final morphology of MOFs, such as shape, average particle size and textural properties. First, this hypothesis was further supported by scanning electron microscopy (SEM)

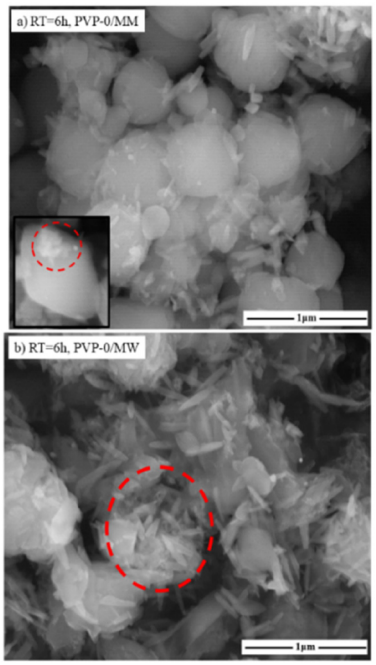

Fig. 3 SEM images of samples synthesized in 6 hours. (a) PVP-0/MM and (b) PVP-0/MW. Circled red dashed lines are representatives of unreacted materials.

images. As shown in the SEM image (Fig. 3a), the particles exhibited a hexagonal bipyramidal shape with smooth edges, consistent with the literature reported for the conventional method.[39] In the PVP-0/MW sample (water post-synthesis treatment), some crystals, like needles, were observed among the particles, highlighted with dashed circles in Fig. 3(a) and (b). These structures were likely residual terephthalic acid that was not completely removed during the post-synthesis treatment. The SEM images showed that the MOF particles, especially in the PVP-0/MW sample, were surrounded by unreacted terephthalic acid (needles). This observation aligns with the XRD results (marked by asterisks in XRD patterns), which showed peaks corresponding to terephthalic acid in the PVP-0/MW sample compared to PVP-0/MM. This further indicates that water was less effective than methanol in removing the unreacted linker.

To further investigate the impact of sonochemical synthesis on particle formation and size, dynamic light scattering (DLS) analysis was performed. According to the DLS results (Fig. 4) the average particle size of the PVP-0/MM and PVP-0/MW samples synthesized *via* ultrasound-assisted methods was below 1 μm, where particle size distributions of previous studies have been reported up to 2 μm for the solvothermal method.[40] The results confirmed that the extreme conditions of ultrasound promoted rapid MOF crystallization and reduced the particle size of MOF-235. Moreover, the results showed a slightly smaller average particle size distribution for the PVP-0/MW sample compared to the PVP-0/MM sample, which is consistent with the XRD and SEM results. This difference can be attributed to the type of solvent used in the post-synthesis

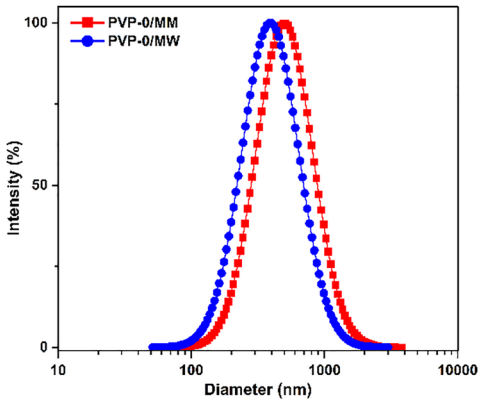

Fig. 4 Particle size distribution by DLS of PVP-0/MM and PVP-0/MW samples synthesized in 6 hours using an ultrasound probe (70 °C).

treatment and the presence of unreacted materials, as discussed in this work.

The specific surface areas of the samples were evaluated using nitrogen-sorption measurement (Fig. 5). Both PVP-0/MM and PVP-0/MW samples exhibited a pattern associated with a combination of type-I and type-IV isotherms, characteristic of microporous and mesoporous structures.[41]

Notably, the PVP-0/MM sample displayed a broader and more pronounced hysteresis loop, suggesting the presence of materials with a combination of rigid and flexible porous structures related to MOF-235 and MIL-53(Fe), respectively. In contrast, the PVP-0/MW sample showed minimal hysteresis, with nearly overlapping adsorption and desorption branches. A slight hysteresis loop was observed around a relative pressure of 0.4 P/P_0, which may suggest the coexistence of both flexible

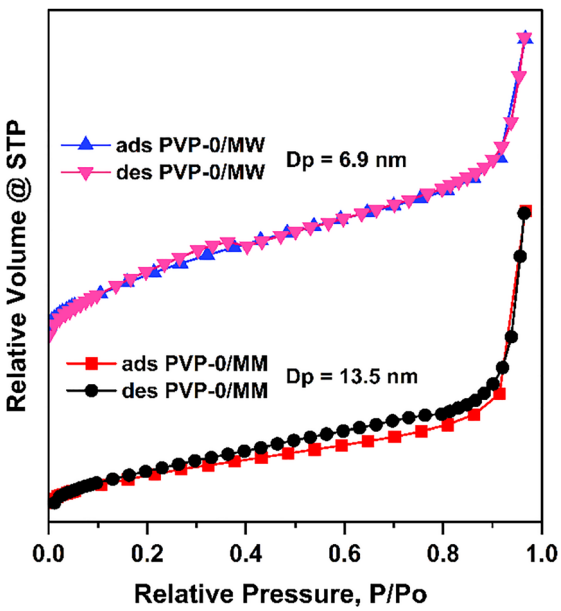

Fig. 5 Nitrogen adsorption–desorption isotherms, (D_p) average pore diameter, as determined using N_2 adsorption–desorption isotherms at 77 K of PVP-0/MM and PVP-0/MW samples synthesized in 6 hours using an ultrasound probe (70 °C).

and rigid pore structures. However, as reported in the previous literature, nitrogen is not a favorable molecule for characterizing flexible porous structures such as MIL-53(Fe).[42] Therefore, the presence of MIL-53(Fe) may not substantially affect the physisorption results of the samples. Consequently, the data on textural properties in this work should be compared with the literature data on MOF-235.

According to the Brunauer–Emmett–Teller (BET) surface area was approximately 24.5 $m^2\ g^{-1}$ for PVP-0/MW and 12.5 $m^2\ g^{-1}$ for PVP-0/MM. The smaller average pore diameter and a higher surface area in the PVP-0/MW sample (Fig. 5) confirmed that the presence of unreacted materials for the water-treated sample, as supported by the other characterization results in this work. Additionally, the nitrogen-sorption measurement results showed using the sonochemical method did not change the textural properties of the samples. For instance, higher porosities for the PVP-0/MW sample than those previously reported for MOF-235 (10–20 $m^2\ g^{-1}$). Besides, the surface area, as the values fall within the wide range (10–710 $m^2\ g^{-1}$) reported in previous studies on MOF-235 synthesized by conventional methods.[39,43]

Therefore, 6 hours of sonochemical synthesis was identified as a suitable reaction time to obtain the crystalline MOF-235 phase. Although the presence of the MIL-53(Fe) structure was also observed in the final product, the 6 hours sonochemical synthesis was appropriate for further experiments. To the best of our knowledge, this represents the first successful synthesis of MOF-235 within 6 hours using an ultrasonic generator at a constant temperature of 70 °C. This approach significantly reduced both the reaction time and temperature, while simultaneously accelerating the process of growth and re-crystallization compared to conventional methods, demonstrating the effectiveness of ultrasound-assisted synthesis for MOF-235 preparation.

Crystallinity and chemical evolution of MOFs with polyvinylpyrrolidone (PVP)

While 6 hours of sonochemical synthesis was an appropriate time to synthesize MOF-235, the final product was a mixture of two different phases, MOF-235 and MIL-53(Fe). MIL-53(Fe) is known as a flexible porous framework and thermodynamically stable structure.[10,11] According to previous literature, the synthesis of MIL-53(Fe) has mostly been reported through methods that require high temperature or long reaction times. However, the knowledge of the phase engineering material suggested that using a modulator could be helpful to solve this problem, to transfer and generate more thermodynamically stable phases during synthesis.[19]

This hypothesis was studied by introducing different amounts of polyvinylpyrrolidone (PVP) as a modulator. Several key structural features of PVP, such as the presence of carboxyl and highly polar amide groups, can collaborate and play a crucial role during the synthesis of metal–organic frameworks (MOFs).[24] To investigate the role of PVP as a modulator in phase transforming and its effect on changing the morphology and textural properties of MOFs, syntheses were conducted

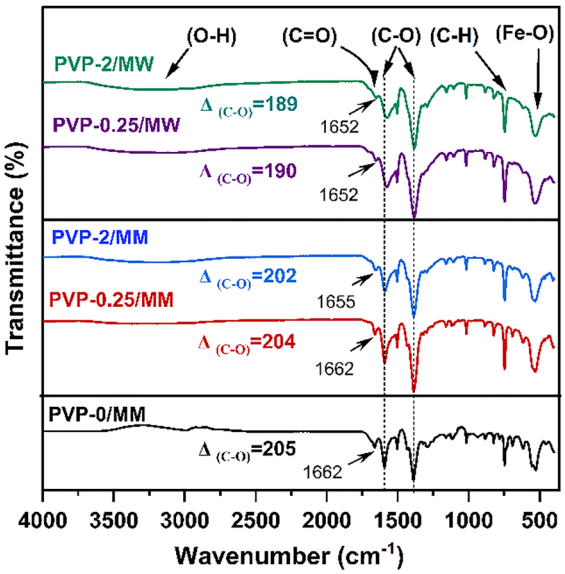

Fig. 6 FTIR spectra of MOF samples synthesized in 6 hours using an ultrasound probe (70 °C). Post-synthesis treatment, the lowest (PVP-0.25) and the highest (PVP-2) molar ratios of PVP. Δ represents the frequency separation between the symmetric (ν_s) and asymmetric (ν_{as}) vibrations of the carboxyl group.

with 0.25, 0.5, 1, 1.5, and 2 molar ratios of PVP. Additionally, the effect of solvents (methanol and water) for post-synthesis treatments was studied.

The purity of the PVP-x samples was assessed by Fourier-transform infrared (FT-IR) spectroscopy in the range of 4000 to 400 cm^{-1}. For conciseness Fig. 6 displays the FTIR spectra of the samples with the lowest PVP-0.25 and the highest PVP-2 molar ratios of PVP for both post-synthesis treatment with methanol and water, compared to the sample without PVP. However, the FTIR spectra of all the samples were provided in the SI.

The observation of the peaks at 550, 750 and 1016 cm^{-1} in all the samples confirmed the preservation of chemical interactions between functional groups similar to the PVP-0/MM sample. The introduction and increasing amount of PVP led to a change in the position of some peaks, such as a slight red shift for the C=O bond from 1662 cm^{-1} to 1566 cm^{-1}. This shift suggested the electron density reduction in the carbonyl bond, reducing its vibration energy. The extent of the red shift was likely attributed to the incorporation of a polymer within the MOF.[44] Moreover, another red shift was observed in the asymmetric (ν_{as}(C–O)) peak, resulting in a narrower frequency separation (Δ) between the symmetric (ν_s) and asymmetric (ν_{as}) vibrations. These changes suggested that an increasing amount of PVP promoted stronger interaction between the polymer and the MOF framework, potentially weakening the bonding between H_2BDC molecules and the metal center. This effect was more noticeable in PVP-*x*/MW samples, likely due to the better removal of residuals during post-synthesis treatment with water, given its higher polarity compared to methanol.

Additionally, previous studies on the MOF-235 structure reported no peaks related to O–H and/or H_2O groups,

consistent with observations in the PVP-0 sample.[12] However, the introduction and increasing the amount of PVP led to the appearance of a broad band between 2500 and 3500 cm^{-1}, related to the O–H group, confirming the presence of PVP in the structure.[24]

The X-ray diffraction (XRD) patterns were performed to evaluate the crystal structure of MOFs with the presence of PVP for 6 hours using the sonochemical method. For clarity and conciseness, Fig. 7 illustrates the XRD patterns belong to the lowest and highest amount of PVP and both post-synthesis treatments, compared to the samples PVP-0. However, the XRD patterns of all the samples are provided in the SI.

According to the XRD patterns, the incorporation of PVP during synthesis led to a gradual reduction in the intensity of the diffraction peaks. Nevertheless, the main diffraction peak at 9.5° remained visible in all the samples, indicating that the preservation of the inherent crystallinity of synthesized particles in the presence of PVP. As the amount of PVP increased, the intensity of the peaks decreased, suggesting that PVP inhibited crystal growth. In other words, at lower PVP concentrations, the carboxyl groups present in its structure, which are similar to those in terephthalic acid, can compete with the ligand for binding sites on the metal centers during synthesis.[18,24] In contrast, at higher PVP concentrations (PVP-2), a more pronounced phase transformation was observed, which more closely resembled the characteristic features of MIL-53(Fe) (CIF: 690316 and 258445).[36,45]

These observations suggested that, alongside the ultrasound conditions that facilitate the crystallization, the incorporation of PVP contributed to the formation of a more thermodynamically stable iron-based MOF phase (MIL-53). Previous studies have shown that increasing precursor concentration can facilitate phase transition.[19] For instance, Bauer *et al.* reported that by increasing the amount of $FeCl_3$ and NH_2–H_2BDC in the solvothermal method, the pure crystal phase of MIL-101-NH_2 (Fe) was converted to MIL-53-NH_2(Fe).[22] Therefore, a higher amount of PVP likely increased the precursor concentration to enhance the formation of the MIL-53(Fe) crystal phase.

Notably, structural changes were more evident when water was used for post-synthetic treatment. The PVP-0.25/MW sample exhibited a significant decrease in peak intensities and a notable shift of the peak from 12.5° to a lower angle. Nevertheless, for methanol-treated samples, the peaks related to MOF-235 were still observed. These differences belonged to the type of solvent of the post-synthesis treatment step. Introducing material with different polarities requires a solvent with an appropriate polarity for effective purification. Safo *et al.* reported the signifying effect of polar solvent in removing the weakly and physisorbed PVP, which was used as a capping agent, during washing the synthesized particles.[44] Thus, water with higher polarity compared to methanol could be more effective for the purification of the samples synthesized with PVP. This enhanced purification enabled more accurate characterization and contributed to the observed phase transformation as previously reported.[13,17]

XRD and FTIR patterns showed that PVP, as a modulator and surfactant, influenced the final crystal structure of MOFs. Moreover, in post-synthesis treatment, the higher polarity of water played an important role in obtaining a higher quality of material for characterization. These findings highlighted the combined effects of synthesis time, modulator presence, and post-synthesis treatment in achieving the final structure closer to the MIL-53 crystal phase.

To confirm the hypothesis related to the contribution of PVP as a modulator and surfactant, scanning electron micrograph (SEM) images and dynamic light scattering (DLS) analysis were conducted. Fig. 8 showed just the combined effect of the lowest and highest amount of PVP and ultrasound on the shape and average particle size of PVP-*x*/MM and PVP-*x*/MW samples for conciseness. However, the SEM images and DLS charts of all the samples were provided in the SI.

According to the SEM images of PVP-*x*/MW and PVP-*x*/MM samples (Fig. 8), the incorporation of PVP during synthesis resulted in more homogeneous particle morphologies and reduced aggregation. Moreover, DLS analysis of the PVP-assisted samples showed that increasing the amount of PVP initially led to a slight increase in the average particle size, followed by a slight decrease at higher concentrations. In contrast, the DLS analysis of the water-treated samples revealed that, higher amount of PVP produced particles with slightly narrower size distributions and greater homogeneity compared to the methanol-treated samples.

SEM images provided further insights to understand the differences in average particle size. It can be seen, PVP-0.25/MM and PVP-2/MM showed the presence of needle-shaped particles among MOF particles (red dashed lines in SEM images (Fig. 8)), reflecting less effectiveness of the solvent in purification. In contrast, PVP-0.25/MW and PVP-2/MW samples exhibited a

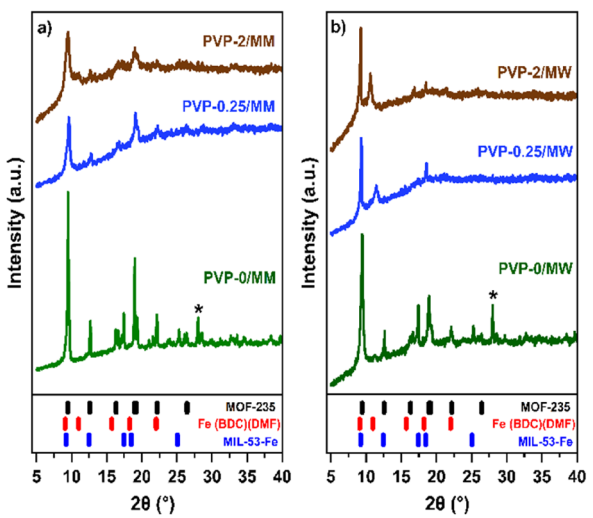

Fig. 7 XRD patterns of MOF samples synthesized in 6 hours under an ultrasound reaction with the lowest (0.25) and the highest (2) molar ratios of PVP at (70 °C) and post-synthesis treatment by (a) methanol and (b) methanol–water. Asterisks mark peaks belonging to the H_2BDC phase.[35] The final Rietveld plots were calculated from CIF files of MOF-235 and two different crystal phases of MIL-53(Fe).[31,36,45]

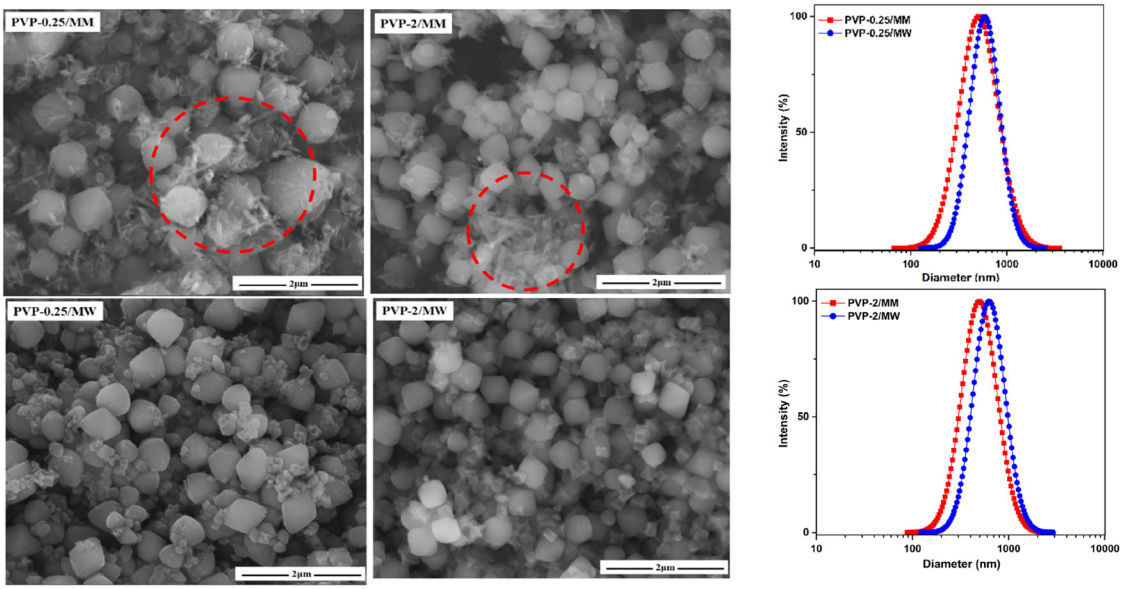

Fig. 8 SEM images and particle size distribution by DLS of the samples with the lowest PVP-0.25/MM, PVP-0.25/MW, and the highest PVP-2/MM and PVP-2/MW molar ratios of PVP synthesized in 6 hours using an ultrasound probe at a constant temperature of 70 °C. Circled red dashed lines are representative of unreacted materials.

lower number of unreacted materials compared to methanol-treated samples, indicating an enhanced purification process during post-synthesis treatment with water.

The interaction of PVP within the MOF structure, due to the presence of amide groups in the PVP structure, which gives PVP high polarity, could change the surface polarity of particles, consequently changing the interaction of the synthesized particles with unreacted materials. In this sense, a highly polar solvent will be more effective for the purification process. Fig. 8 demonstrates that less agglomeration existed when the particles were surrounded by unreacted materials. Therefore, water, as a highly polar solvent, played a crucial role in post-synthesis treatment, facilitating the removal of unreacted ligands and residuals trapped inside the pores or among particles during synthesis.

These observations indicate that the broader lognormal particle size distribution observed in the methanol-treated samples suggest lower effectiveness of methanol compared to water in the purification step. This trend is consistent with the FTIR and XRD results, which highlight structural differences between MOFs synthesized with PVP with different post-synthesis treatment. Therefore, PVP not only acted as a modulator to influence particle size but also served as a surfactant, functioning as a stabilizing agent and enhancing purification efficiency when water was used in the post-synthesis treatment.

The evaluation of specific surface areas and pore size distributions of the samples synthesized with PVP under sonochemical synthesis conditions was investigated by using nitrogen-sorption measurement. Due to the minor differences observed between the surface areas of the PVP-0.25 and PVP 0.5 samples compared to the sample without PVP (PVP-0), only the physisorption isotherms of the samples prepared with 1.0, 1.5,

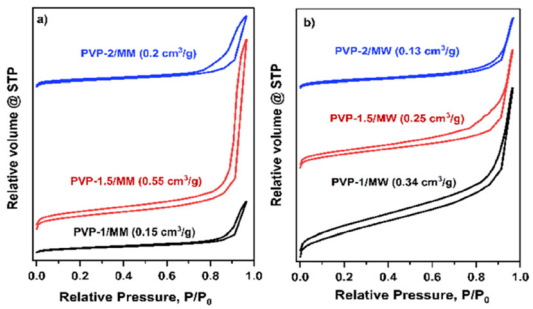

Fig. 9 The nitrogen adsorption–desorption isotherms of the samples with the 1, 1.5 and 2 PVP molar ratios, synthesized in 6 hours using an ultrasound probe at a constant temperature of 70 °C and post-synthesis treatment with (a) methanol and (b) methanol–water. The total pore volume is shown in parentheses.

and 2.0 molar ratios of PVP are presented in Fig. 9(a) and (b) for clarity. However, the surface area and pore size distribution data for all samples are available in the SI. Additionally, the detailed textural parameters are summarized in Table 1.

Incorporation of PVP significantly influences the textural properties of the samples, leading to a notable increase in surface area and porosity. Progressive increase of BET surface area and total pore volume, reaching a maximum for PVP-1.5/MM and PVP-1/MW samples. A clear difference was observed where hysteresis behavior appeared upon PVP introduction, which became more significant with increasing the amount of PVP. According to previous studies, large hysteresis could be a result of the flexible porous structure of MOF, such as MIL-53(Fe), which involves structural transitions on adsorption and desorption.[11,46] The hysteresis observed in the results likely suggested that PVP incorporation, besides ultrasound synthesis,

Table 1 Textural properties[a] of MOF samples synthesized by 6 hours with different amounts of PVP using an ultrasound probe (70 °C) calculated from N_2 adsorption desorption isotherms

Sample	S_{BET} ($m^2\ g^{-1}$)	D_p (nm)	Sample	S_{BET} ($m^2\ g^{-1}$)	D_p (nm)
PVP-0 MM	12.53	13.55	PVP-0 MW	24.47	6.92
PVP-0.25 MM	22.18	10.04	PVP-0.25 MW	23.96	12.08
PVP-0.5 MM	17.16	16.34	PVP-0.5 MW	49.69	11.31
PVP-1 MM	36.55	15.42	PVP-1 MW	188.07	7.17
PVP-1.5 MM	169.64	12.99	PVP-1.5 MW	134.18	7.18

[a] Specific BET surface area (S_{BET}) and average pore diameter (D_p) as determined by N_2 adsorption–desorption isotherms at 77 K.

induced structural flexibility and transformed the rigid MOF-235 framework into a flexible form of MIL-53(Fe). Additionally, the presence of hysteresis in samples synthesized with PVP could also indicate the formation of mesopores, consistent with the pore size distribution analysis, which showed a shift from small pores to higher size pores, toward a narrower mesopore range (SI).[47]

On the other hand, with the cooperation of the highest amount of PVP in both samples, the surface area and porosity of the samples were reduced. According to the literature, MIL-53(Fe) synthesis by the conventional method typically has shown a low or negligible accessible surface area or pore volume.[48] This finding aligns with our XRD discussion, suggesting that the reduction in surface area and porosity correlates with increased formation of the MIL-53(Fe) structure. Specifically, this reduction appeared in the PVP-1.5/MW and PVP-2/MW samples, which also underwent more thorough purification with water to better remove the unreacted materials.

Effective purification is essential to fully access the pore structure of MOFs, as it requires the removal of residual solvents and other trapped species, as reported by Otun K.[49] Post-synthesis treatment with a polar solvent has been identified as an effective method for eliminating residual species.[50] Previous studies indicate that the $[FeCl_4]^-$ counterion plays a crucial role in the formation of MOF-235(Fe).[31] After recrystallization of MIL-53(Fe), the counterion, as a residual species, can be trapped within the MOF framework.

Therefore, the use of water as a highly polar solvent enhanced the porosity of particles by better removing trapped counterions and other impurities.

These findings confirmed that PVP plays a dual role in both the particle properties and the phase transition of the structure from MOF-235 to MIL-53. The lower amount of PVP contributed to increased surface area by reducing the average particle size and hindering crystal growth, while a higher amount of PVP acted as a modulator and led to the phase transition to a higher thermodynamic structure. Overall, the cooperation of PVP besides the ultrasound synthesis method led to phase transition and pore structure modification. PVP increased the surface area, induced structural flexibility, and enhanced *meso*-porosity, making it an effective modulator and surfactant to improve the textural properties of the sonochemical synthesized MOFs.

Conclusions

This study presented the first report of a rapid and effective strategy for synthesizing MOF-235 and inducing its phase transformation to a more thermodynamically stable structure, MIL-53(Fe), *via* a sonochemical method. The synthesis was achieved within 6 hours at a constant temperature of 70 °C. The rapid vibration of the ultrasound probe causes cavitation, releasing intense localized energy that facilitates nucleation and crystallization. Although both MOF-235 and MIL-53(Fe) phases coexisted in the final product, the presence of polyvinylpyrrolidone K30 (PVP) as a modulator steered the reaction toward the formation of MIL-53(Fe), the more thermodynamically favored phase.

The characterization techniques, including XRD, FTIR, SEM, DLS, and nitrogen adsorption–desorption analysis, revealed that PVP significantly played important roles as a modulator and surfactant. PVP, besides the sonochemical method, influenced the particle morphology, size distribution, and textural properties, notably increasing the surface area up to 188 $m^2\ g^{-1}$.

The importance of purification was further demonstrated through post-synthesis treatment using methanol and water as solvents. The high polarity of water for the purification of PVP-containing samples proved more effective than methanol to remove unreacted materials.

This study presented the first report on the use of ultrasound-assisted synthesis for MOF-235 incorporation of PVP. The results emphasized the critical role of modulators in changing MOF structures and demonstrated how post-synthesis treatments and solvent choice significantly influenced the quality of synthesized MOF. Overall, this work offers valuable insights into the transformation of MOF-235 to MIL-53 phases, laying the groundwork for tailoring MOF properties to meet specific application requirements across various fields.

AI tools

Prior to submission, grammatical mistakes were checked and amended using the Grammarly tool and ChatGPT.

Author contributions

All the authors contributed equally.

Conflicts of interest

There are no conflicts to declare.

Data availability

The crystallographic data (CIF files) used for three-dimensional visualization and morphology analysis were sourced from the Cambridge Crystallographic Data Centre (CCDC) and can be accessed using the following accession numbers: MOF-235 (CCDC 255079) and MIL-53(Fe) (CCDC 690316 and 258445),

available online at https://www.ccdc.cam.ac.uk/. These files were calculated using VESTA 3 software. Graphs and charts were prepared using OriginPro 2024b. No additional software, code, or external data repositories were used in this study.

Supporting information is available. See DOI: https://doi.org/10.1039/d5ma00699f.

Acknowledgements

The authors would like to thank Secretaría de Ciencia, Humanidades, Tecnología e Innovación (SECIHTI) from Mexico for the financial support (grant no. 2022-000002-01NACF-03589).

Notes and references

1 S. M. Moosavi, A. Nandy, K. M. Jablonka, D. Ongari, J. P. Janet, P. G. Boyd, Y. Lee, B. Smit and H. J. Kulik, *Nat. Commun.*, 2020, **11**, 4068.
2 B. P. Carpenter, A. R. Talosig, B. Rose, G. Di Palma and J. P. Patterson, *Chem. Soc. Rev.*, 2023, **52**, 6918–6937.
3 D. Chakraborty, A. Yurdusen, G. Mouchaham, F. Nouar and C. Serre, *Adv. Funct. Mater.*, 2023, **34**(43), 2309089.
4 M. D. Allendorf, V. Stavila, M. Witman, C. K. Brozek and C. H. Hendon, *J. Am. Chem. Soc.*, 2021, **143**(18), 6705–6723.
5 R. Zhu, M. Cai, T. Fu, D. Yin, H. Peng, S. Liao, Y. Du, J. Kong, J. Ni and X. Yin, *Pharmaceutics*, 2023, **15**, 1599.
6 C. Tamames-Tabar, D. Cunha, E. Imbuluzqueta, F. Ragone, C. Serre, M. J. Blanco-Prieto and P. Horcajada, *J. Mater. Chem. B*, 2014, **2**, 262–271.
7 P. Horcajada, C. Serre, M. Vallet-Regí, M. Sebban, F. Taulelle and G. Férey, *Angew. Chem., Int. Ed.*, 2006, **45**, 5974–5978.
8 X. Liu, Y. Zhou, J. Zhang, L. Tang, L. Luo and G. Zeng, *ACS Appl. Mater. Interfaces*, 2017, **9**, 20255–20275.
9 Z. Jiang, Y. Zheng, L. Zhang, L. Xu, Q. Feng, C. Luo, W. Tan and J. Wang, *Int. J. Hydrogen Energy*, 2024, **82**, 703–712.
10 G. Férey and C. Serre, *Chem. Soc. Rev.*, 2009, **38**, 1380–1399.
11 F. Millange and R. I. Walton, *Isr. J. Chem.*, 2018, **58**, 1019–1035.
12 F. Millange, M. I. Medina, N. Guillou, G. Férey, K. M. Golden and R. I. Walton, *Angew. Chem.*, 2010, **122**, 775–778.
13 D. Bara, E. G. Meekel, I. Pakamore, C. Wilson, S. Ling and R. S. Forgan, *Mater. Horiz.*, 2021, **8**, 3377.
14 B. Achenbach, A. Yurdusen, N. Stock, G. Maurin and C. Serre, *Adv. Mater.*, 2025, 2411359.
15 E. Haque, N. A. Khan, H. J. Park and S. H. Jhung, *Chem. – Eur. J.*, 2010, **16**, 1046–1052.
16 J. Gordon, H. Kazemian and S. Rohani, *Microporous Mesoporous Mater.*, 2012, **162**, 36–43.
17 R. S. Forgan, *Commun. Mater.*, 2024, **5**, 46.
18 C. R. Marshall, S. A. Staudhammer and C. K. Brozek, *Chem. Sci.*, 2019, **10**(41), 9396–9408.
19 Q. Yun, Y. Ge, Z. Shi and J. Liu, *Chem. Rev.*, 2023, **123**, 13489–13692.
20 C. R. Marshall, E. E. Timmel, S. A. Staudhammer and C. K. Brozek, *Chem. Sci.*, 2020, **11**(42), 11539–11547.
21 K. Li, J. Yang and J. Gu, *Chem. Sci.*, 2019, **10**(22), 5743–5748.
22 S. Bauer, C. Serre, T. Devic, P. Horcajada, J. Marrot, G. Férey and N. Stock, *Inorg. Chem.*, 2008, **47**, 7568–7576.
23 J. Łuczak, M. Kroczewska, M. Baluk, J. Sowik, P. Mazierski and A. Zaleska-Medynska, *Adv. Colloid Interface Sci.*, 2023, **314**, 102864.
24 K. M. Koczkur, S. Mourdikoudis, L. Polavarapu and S. E. Skrabalak, *Dalton Trans.*, 2015, **44**, 17883–17905.
25 A. Li, X. Yang and J. Chen, *RSC Adv.*, 2021, **11**, 10540–10547.
26 Y. Wang, C. Yang, C. Zhang, M. Duan, H. Wang, H. Fan, Y. Li, J. Shangguan and J. Lin, *Fuel*, 2022, **319**, 123845.
27 Z. Yu, M. Lepoitevin and C. Serre, *Adv. Healthcare Mater.*, 2025, **14**, 2402630.
28 W. J. Son, J. Kim, J. Kim and W. S. Ahn, *Chem. Commun.*, 2008, 6336–6338.
29 T. Chalati, P. Horcajada, R. Gref, P. Couvreur and C. Serre, *J. Mater. Chem.*, 2011, **21**, 2220–2227.
30 J. Amaro-Gahete, R. Klee, D. Esquivel, J. R. Ruiz, C. Jiménez-Sanchidrián and F. J. Romero-Salguero, *Ultrason. Sonochem.*, 2019, **50**, 59–66.
31 A. C. Sudik, A. P. Côté and O. M. Yaghi, *Inorg. Chem.*, 2005, **44**, 2998–3000.
32 D. L. Pavia, G. M. Lampman, G. S. Kriz and J. R. Vyvyan, *Introduction to spectroscopy*, 2013.
33 M. D. Lind, *J. Chem. Phys.*, 1967, **47**, 990–993.
34 M. Bailey and C. J. Brown, *Acta Crystallogr.*, 1967, **22**(3), 387–391.
35 J. G. Flores, R. Delgado-García and M. Sánchez-Sánchez, *Catal. Today*, 2022, **390–391**, 237–245.
36 F. Millange, N. Guillou, R. I. Walton, J. M. Grenèche, I. Margiolaki and G. Férey, *Chem. Commun.*, 2008, 4732–4734.
37 K. Matuszek, E. Pankalla, A. Grymel, P. Latos and A. Chrobok, *Molecules*, 2019, **25**(1), 80.
38 K. S. Suslick, D. A. Hammerton and R. E. Cline, *J. Am. Chem. Soc.*, 1986, **108**, 5641–5642.
39 S. C. Moore and M. L. Sarazen, *AIChE J.*, 2023, **69**, e18205.
40 L. P. Camargo, P. R. C. da Silva, A. Batagin-Neto, V. Klobukoski, M. Vidotti and L. H. Dall'Antonia, *Appl. Mater. Today*, 2022, **28**, 101540.
41 M. Thommes, K. Kaneko, A. V. Neimark, J. P. Olivier, F. Rodriguez-Reinoso, J. Rouquerol and K. S. W. Sing, *Pure Appl. Chem.*, 2015, **87**, 1051–1069.
42 D. Villarroel-Rocha, J. Villarroel-Rocha, S. Amaya-Roncancio, C. García-Carvajal, D. A. Barrera, J. Arroyo-Gómez, D. A. Torres-Ceron, E. Restrepo-Parra and K. Sapag, *ACS Omega*, 2024, **9**, 21930–21938.
43 C. Rui Xie, Y. Xuan Song, G. Yang, C. Gong Sun, X. Luo and T. Wu, *Mater. Today Commun.*, 2024, **41**, 110843.
44 I. A. Safo, M. Werheid, C. Dosche and M. Oezaslan, *Nanoscale Adv.*, 2019, **1**, 3095–3106.
45 T. R. Whitfield, X. Wang, L. Liu and A. J. Jacobson, *Solid State Sci.*, 2005, **7**, 1096–1103.

46 S. Krause, N. Hosono and S. Kitagawa, *Angew. Chem., Int. Ed.*, 2020, **59**, 15325–15341.
47 A. Schneemann, V. Bon, I. Schwedler, I. Senkovska, S. Kaskel and R. A. Fischer, *Chem. Soc. Rev.*, 2014, **43**, 6062–6096.
48 P. Horcajada, C. Serre, G. Maurin, N. A. Ramsahye, F. Balas, M. Vallet-Regí, M. Sebban, F. Taulelle and G. Férey, *J. Am. Chem. Soc.*, 2008, **130**, 6774–6780.
49 K. O. Otun, *Inorg. Chim Acta*, 2020, **507**, 119563.
50 H. Molavi and M. S. Salimi, *Sci. Rep.*, 2025, **15**, 7074.